Journal of Power Sources 580 (2023) 233298

Contents lists available at ScienceDirect

Journal of Power Sources

journal homepage: www.elsevier.com/locate/jpowsour

Functionalized Hf_3C_2 and Zr_3C_2 MXenes for suppression of shuttle effect to enhance the performance of sodium–sulfur batteries

Saba Khan [a,b], Narender Kumar [a,b], Tanveer Hussain [c], Nacir Tit [a,b,*]

[a] Department of Physics, UAE University, P.O. Box 15551, Al-Ain, United Arab Emirates
[b] National Water and Energy Center, UAE University, P.O. Box 15551, Al-Ain, United Arab Emirates
[c] School of Science and Technology, University of New England, Armidale, New South Wales, 2351, Australia

HIGHLIGHTS

- DFT study of suppression of shuttle effect in NaSBs proposed new cathode additives.
- 4 MXenes ($Hf_3C_2T_x$, $Zr_3C_2T_x$, T = F/O) were considered as cathode additives.
- E_{bind} of Na_2S_n with MXenes stronger than electrolyte so to prevent shuttle effect.
- They have moderate potential barrier for easy dissociation of Na_2S during charging.
- $Zr_3C_2O_2$ MXenes found to be the best for performance and lifetime of the NaSBs.

GRAPHICAL ABSTRACT

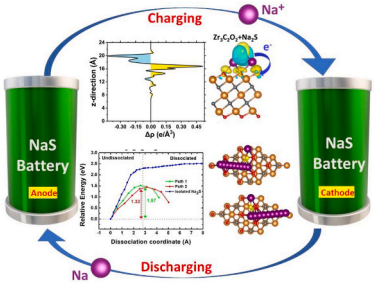

ARTICLE INFO

PACS Numbers:
31.15.E-
68.43.-h
68.43.Mn
68.47.Fg
71.15.Nc
73.20.At
81.05.ue

Keywords:
Sodium-sulfur batteries
DFT
Chemisorption/physisorption: Adsorbates on surfaces
MXenes
Energy storage

ABSTRACT

Sodium-sulfur batteries show great potential for storing large amounts of energy due to their ability to undergo a double electron-redox process, as well as the plentiful abundance of sodium and sulfur resources. However, the shuttle effect caused by intermediate sodium polysulfides (Na_2S_n) limits their performance and lifespan. To address this issue, here we propose using $Hf_3C_2T_2$ and $Zr_3C_2T_2$ (T = F, O), two functionalized MXenes, as cathode additives to suppress the shuttle effect. By using density-functional theory calculations, we investigate nature of the interactions between Na_2S_n and MXene, such as the strength of adsorption energy, the electronic density of states, the charge exchange, and the dissociation energy of the Na_2S molecule. Our findings show that both $Hf_3C_2T_2$ and $Zr_3C_2T_2$ systems inhibit the shuttle effect by binding to Na_2S_n with a binding energy stronger than the commonly used electrolyte solvents. These MXenes retain their metallicity during this process and the decomposition barrier for Na_2S_n on the oxygen-functionalized MXenes gets reduced which enhances the electrochemical process. Among the MXene systems studied, $Zr_3C_2O_2$ shows the best performance in suppressing the shuttle effect and catalyzing the electrochemistry process and, thus, increasing the battery's reversible capacity and lifespan.

* Corresponding author. Department of Physics, UAE University, P.O. Box 15551, Al-Ain, United Arab Emirates.
E-mail address: ntit@uaeu.ac.ae (N. Tit).

https://doi.org/10.1016/j.jpowsour.2023.233298
Received 22 February 2023; Received in revised form 8 May 2023; Accepted 5 June 2023
Available online 19 June 2023

Table 1
The lattice constants and geometrical parameters for $Hf_3C_2T_2$ and $Zr_3C_2T_2$ with passivations T = F, O. Theoretical results are compared to the available experimental data.

MXene	Hf_3C_2		Zr_3C_2	
Passivation	Passivation F	Passivation O	Passivation F	Passivation O
Lattice Constant DFT	3.291 Å	3.269 Å	3.342 Å	3.319 Å
Lattice Constant Exp.	3.290 Å(*)	3.27 Å(*)	3.332 Å(**)	3.314 Å(**)
Geometry	$b_{C\text{-}Hf}$ = (2.19, 2.37) Å $b_{Hf\text{-}F}$ = 2.319 Å Slab thickness = 7.66 Å Ang C = 87.1° Ang Hf = 90.59°	$b_{C\text{-}Hf}$ = (2.36, 2.32) Å $b_{Hf\text{-}O}$ = 2.105 Å Slab thickness = 7.32 Å Ang C = 90.54° Ang Hf = 91.63°	$b_{C\text{-}Zr}$ = (2.23, 2.38) Å $b_{Zr\text{-}F}$ = 2.333 Å Slab thickness = 7.75 Å Ang C = 87.50° Ang Zr = 90.89°	$b_{C\text{-}Zr}$ = (2.36, 2.34) Å $b_{Zr\text{-}O}$ = 2.319 Å Slab thickness = 7.43 Å Ang C = 90.90° Ang Zr = 90.03°

(*) Reference [32].
(**) Reference [33].

1. Introduction

Portable electronic devices and electric vehicles have heavily relied upon lithium-ion batteries (LIBs) as the main energy storage technology in the past few decades [1–3]. However, the sustainability of lithium resources is a growing concern due to their depletion from the earth's crust caused by high consumption rates. In response, alternative batteries based on other materials have been investigated, including sodium-ion [4], potassium-ion [5], aluminum-ion [6], zinc-air [7], and sodium-sulfur batteries (NaSBs) [8,9]. NaSBs have received a lot of attention from researchers due to their high energy density and reliability at room temperature, and the fact that both sodium and sulfur are abundantly available in nature, making them a more sustainable option than LIBs [8,9].

The performance of NaSB's is negatively impacted at higher temperatures because the energy density gets reduced due to the formation of NaS_2 instead of Na_2S_2 [10,11]. Even at room temperature, the performance of NaSBs is limited by several factors, including poor cycling stability due to the reduction in the electrical conductivity and the volumetric expansion of the sulfur cathode [12]. The main reason of these shortcomings is attributed to the transformation of sulfur to sodium polysulfides (Na_2S_n), which is a recurring process resulting in the dissolution of Na_2S_n in common electrolyte solvents such as 1,2-dimethoxyethane (DME) and 1,3-dioxolane (DOL). This phenomenon, known as the shuttle effect, leads to the gradual depletion of cathode material and anode passivation and, consequently, gradual reduction in the performance and shortening in the lifetime [9,13].

Targetting the effective suppression of the shuttle effect in NaSBs, many researchers shared the idea of physical confinement and chemical adsorption but through different strategies [9,13]. The idea of chemical adsorption of Na_2S_n requires the insertion of an additive-cathode to play the role of an anchoring material. In literature, many anchoring materials have been proposed, ranging from (i) graphene/N-doped carbon [14], to (ii) MOF-derived S, O and N-doped porous carbon [15–17], to (iii) MN4-doped graphene (M = Cr, Mn, Fe, Co, Cu) [18], to (iv) CoP–Co composite [19], to (v) C_2N monolayer (ML) [20], to (vi) As_2S_3 ML [21], to (vii) an effective sulfiphilic host with gold nanodots decorated on hierarchical N-doped carbon microspheres (NC/Au/S) [22], and to (viii) functionalized MXenes monolayer (ML) [23–26]. It is worth to emphasize that the role of the additive anchoring electrode is to prevent the dissolution of Na_2S_n in the electrolyte during the battery's discharging phase. So, it must provide a chemical binding with Na_2S_n stronger than those with the electrolytes. On the other hand, these interactions should not be too strong to restrict the reversibility of Na_2S_n during the charging process. Meanwhile, another role of the anchoring material is to enhance the electrical conductivity of the sulfur cathode.

The first successful synthesis of MXenes (e.g., Ti_3AlC_2) [27] and functionalized MXenes (e.g., $Ti_3C_2T_x$) [28] has offered a novel 2D materials with distinct characteristics. MXenes are usually metallic but their electronic properties could be tuned based upon the passivation with various functional groups, such as oxygen, sulfur, and halogenes (i.e., group VI or VII). So, MXenes have the ability to maintain their

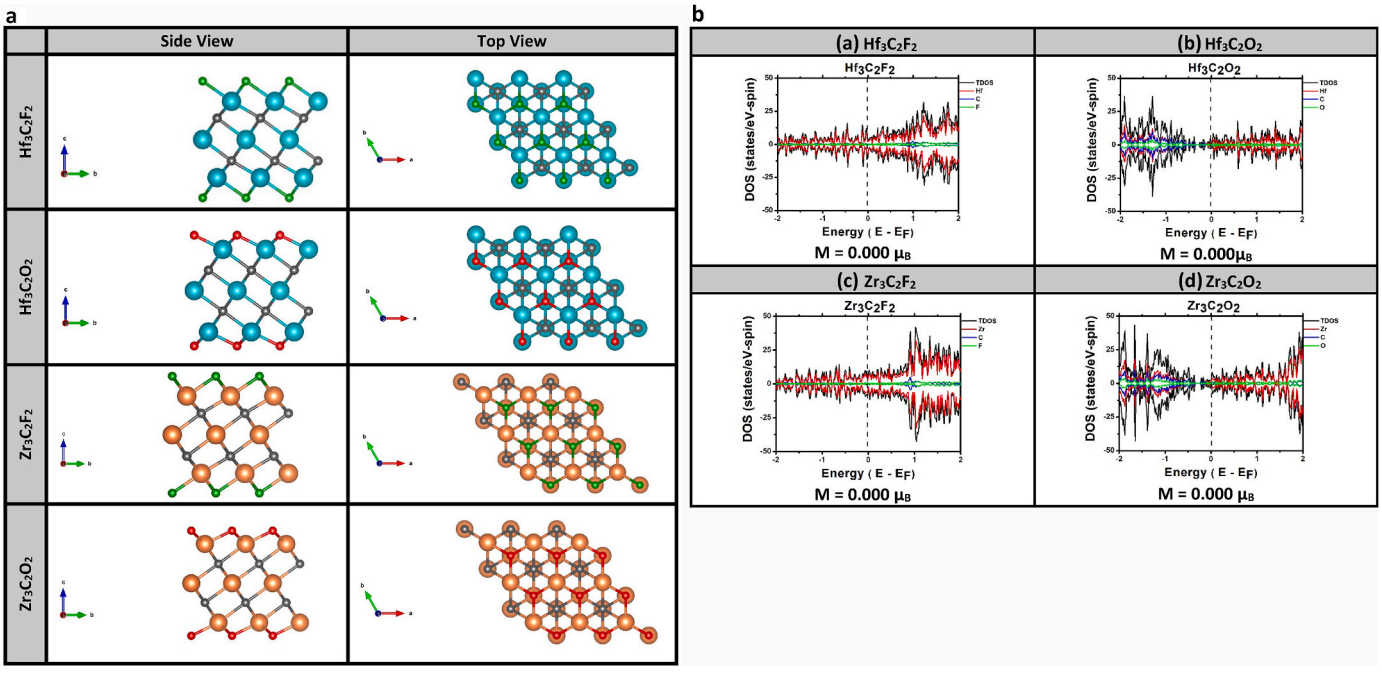

Fig. 1. (a) Side and top views of crystal structures of 4 studied functionalized MXenes $Hf_3C_2T_2$ and $Zr_3C_2T_2$ (T = F,O) using a computational supercell of size 3 × 3 primitive cells. (b) Spin-polarized PDOS and TDOS of MXene monolayers corresponding to part (a).

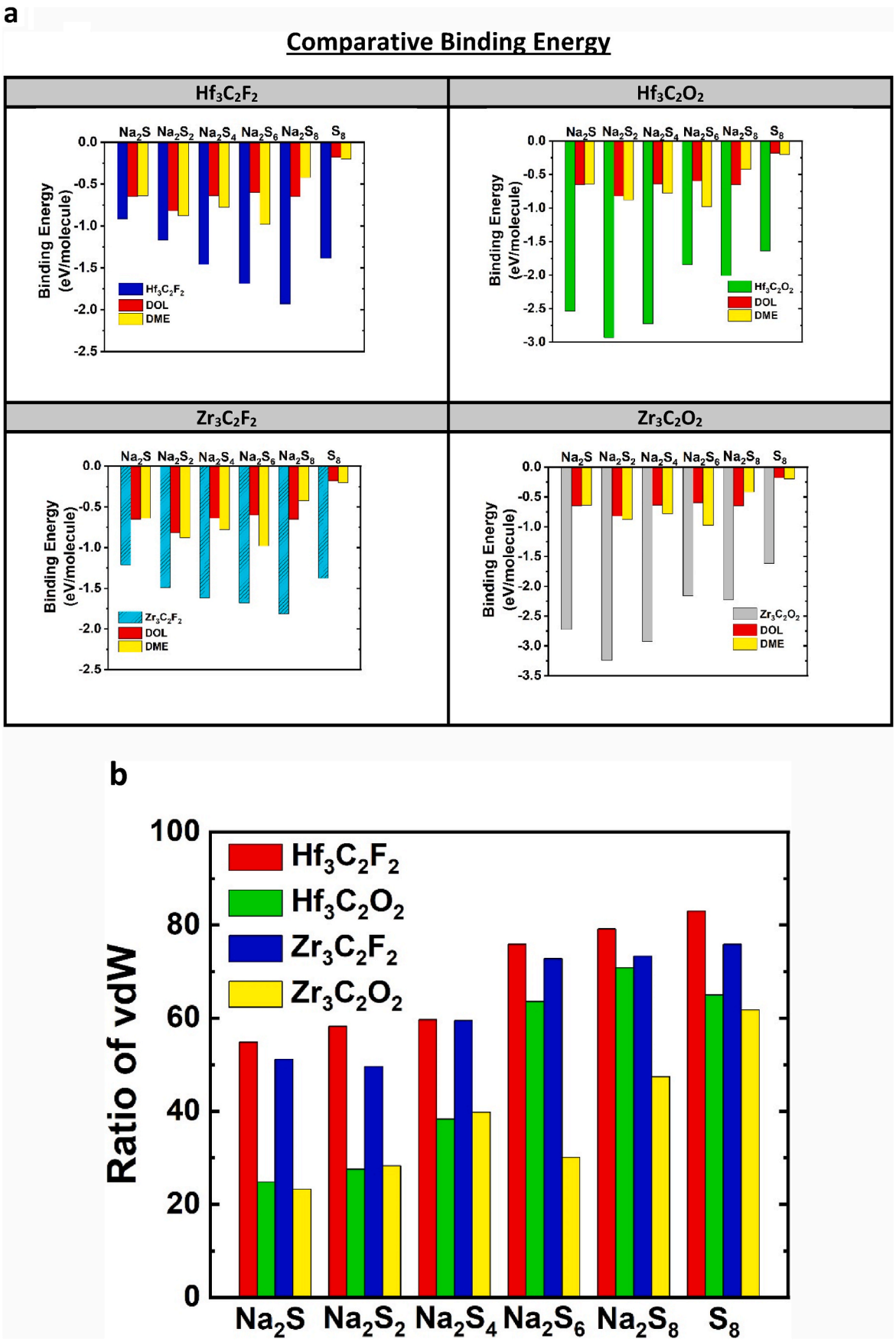

Fig. 2. (a) Binding energies of sodium polysulfides (Na_2S_n) adsorbed on surfaces of 4 MXenes $Hf_3C_2T_2$ and $Zr_3C_2T_2$ (T = F,O). (b) Ratio of contribution of vdW interactions to the adsorption energies of part (a).

Table 2
Calculated binding energies for 6 sodium polysulfides (Na_2S_n) deposited on surfaces of 4 functionalized MXenes $Hf_3C_2T_2$ and $Zr_3C_2T_2$ (T = F,O) and electrolytes (DOL and DME). Benchmarking of our results to others reported in literature is also displayed.

System	Na_2S	Na_2S_2	Na_2S_4	Na_2S_6	Na_2S_8	S_8	Reference
$Hf_3C_2F_2$	−0.92	−1.17	−1.46	−1.69	−1.93	−1.38	This work
$Hf_3C_2O_2$	−2.53	−2.93	−2.73	−1.84	−2.01	−1.64	This work
$Zr_3C_2F_2$	−1.21	−1.49	−1.62	−1.68	−1.81	−1.37	This work
$Zr_3C_2O_2$	−2.73	−3.24	−2.92	−2.16	−2.23	−1.62	This work
DOL	−0.65	−0.82	−0.64	−0.60	−0.65	−0.18	Ref. [16]
DME	−0.64	−0.88	−0.78	−0.98	−0.42	−0.20	Ref. [16]
Graphene	−0.82	−0.67	−0.51	−0.43	−0.33	–	Ref. [16]
N-NPG	−2.77	−1.77	−1.37	−1.43	−1.66	−0.76	Ref. [16]
FeN_4@graphene	−1.09	−1.36	−1.07	−1.16	−1.35	–	Ref. [18]
$Ti_3C_2T_x$ (S-terminated)	–	−1.89	−2.88	−4.72	–	–	Ref. [23]
$Ti_3C_2F_2$	−1.72	−2.06	−1.36	−1.06	−1.54	−0.93	Ref. [25]
$Ti_3C_2O_2$	−3.08	−3.62	−2.18	−2.06	−2.56	−1.20	Ref. [25]
CoP–Co	−1.66	−1.74	−2.43	−2.66	–	–	Ref. [19]
C_2N	−3.09	−3.13	−2.51	−2.39	−2.33	–	Ref. [20]
As_3S_3	−3.26	−2.41	−1.94	−1.49	−1.52	–	Ref. [21]

interactions with most of the molecules at the intermediate strength within the range between strong physisorption and weak chemisorption, which is beneficial to be explored in fabricating reusable biosensors [29,30]. As far as the NaSBs are concerned, the experimental work of Bao and Gogotsi et al. [23] showed that sulfur-doped $Ti_3C_2T_x$ MXenes can inhibit the shuttle effect and maintain the reversible capacity of 577 $mAhg^{-1}$ at 2 °C after 500 cycles. Furthermore, owing to their huge diversity, outstanding metallic conductivity, tunable surface chemistry, and 2D layered structure, MXenes exhibit enormous potential which can be explored for battery applications in general and NaSBs in particular [23–26]. Recent review by Liu and coworkers [31] presented another experimental contribution showing the optimization of electrolyte in enabling the best sulfur redox processes at room temperature (RT) in NaSBs.

Recently, new $Hf_3C_2T_2$ MXenes were successfully synthesized by the group of Zhou and coworkers [32]. These authors showed the potentials of MXenes for lithium and sodium ion batteries with reversible volumetric capacities of 1567 and 504 mAh cm^{-3}, respectively. The same group [33] also reported the successful synthesis of $Zr_3C_2T_x$ and showed them to be more stable than $Ti_3C_2T_x$ at high temperature. Based on these successes, in the present investigation, we aim in developing a superior anchoring material to improve the performance of NaSBs in both perspectives of inhibiting the shuttle effect (during discharging phase) and catalyzing the electrochemistry process (during charging phase). In contrast to many MXenes (e.g., $Ti_3C_2T_x$) presented in literature, the novelty of our work is to assess the mutual effects of both changing the metal and functionalization groups on the interactions with Na_2S_n and compare the results with other anchoring materials previously reported in literature.

2. Computational model and method

In crystalline structure, $M_3X_2T_x$ MXenes are layered hexagonal (belonging to the space group $P6_3/mmc$) [34], with two formula units per primitive cell. So, as a model, we considered a computational supercell of size 3 × 3 primitive cells (i.e., containing 63 atoms). Such a supercell would be sufficient to investigate the adsorption properties of Na_2S_n (n = 1, 2, 4, 6, 8) on $Hf_3C_2T_2$ and $Zr_3C_2T_2$ (T = F, O). One should expect the computations to be spin-polarized and rather demanding as they involve heavy transition metal elements (Hf and Zr), where f-electrons should be included in the calculations. The relaxed atomic structures will be discussed in the next section. To create a periodic slab that does not interact with its mirror images along the z-direction, the supercell dimensions are established as (A = B,C), with A being equal to 3 times the lattice constant indicated in Table 1. A and B are configured to generate the periodic slab in the xy-direction, while C is set to 20 Å, which is sufficiently large to maintain the slab's isolation.

Regarding the method of computation, we employed the latest density-functional theory (DFT), which was integrated into the "Vienna Ab-initio Simulation Package" (VASP) [35]. The projected augmented wave (PAW) method is utilized to handle the interaction between ions and electrons [35]. The Perdew-Burke-Ernzerhof (PBE) functional, together with the generalized gradient approximation (GGA), was utilized to handle the exchange and correlation interactions [36]. We used an energy cut-off of 500 eV. In sampling the Brillouin zone, a k-mesh of 5 × 5 × 1 (12 × 12 × 1) under Monkhorst-Pack scheme [37] was utilized for geometry optimization (DOS calculations). We took as convergence criteria of 10^{-6} eV and 10 meV/Å for total energy and force per atom, respectively. Furthermore, it is crucially important to incorporate the van der Waals (vdW) interactions as they alter the adsorption of Na_2S_n. The vdW interactions are included using the DFT-D3 method of Grimme scheme [38]. The transfer of charge between the adsorbed Na_2S_n and MXene is determined using the Bader charge analysis, which is incorporated within the VASP package [39].

3. Results and discussion

3.1. Structural and electronic properties

In any DFT study, the first step is always the atomic relaxation. Fig. 1a presents the optimized geometries of the four MXenes structures, which include $Hf_3C_2F_2$, $Hf_3C_2O_2$, $Zr_3C_2F_2$, and $Zr_3C_2O_2$ monolayers. Table 1 summarizes all the corresponding parameters. The bond lengths between the passivated F(O) atom and the inner two metal Hf/Zr atoms are presented as b(F–Hf) = 2.319 Å, b(O–Hf) = 2.105 Å, b(F–Zr) = 2.333 Å, and b(O–Zr) = 2.134 Å. The obtained lattice parameters for each structure are also reported and found to be consistent with the experimental [32,33] and the ab-initio results [40,41]. The bond angles of both metal (Hf, Zr) and carbon atoms are about 90°, which is consistent with the previous literature reports [32,33,40,41].

Because transition-metal atoms are present in the composition of these MXenes, it is necessary to include spin-polarization in the electronic structures. The image shown in Fig. 1b illustrates the predicted spin-polarized density of states (PDOS) for $Hf_3C_2X_2$ and $Zr_3C_2X_2$ (where X can be either F or O) based on GGA-PBE calculations. The energy at the Fermi level, which is $E_F = 0$, is used as a reference point. The total density of states (TDOS) and PDOS are displayed for an energy range of [−2,+2] eV around the Fermi level. The results indicate that all four MXenes are paramagnetic metals, which means that the PDOSs of the spin up and the spin down states are identical, resulting in disappearing magnetization, M = 0, and exhibit a finite value at the Fermi energy. The origins of this metallicity can be primarily attributed to the d states of the metal atoms (Hf/Zr).

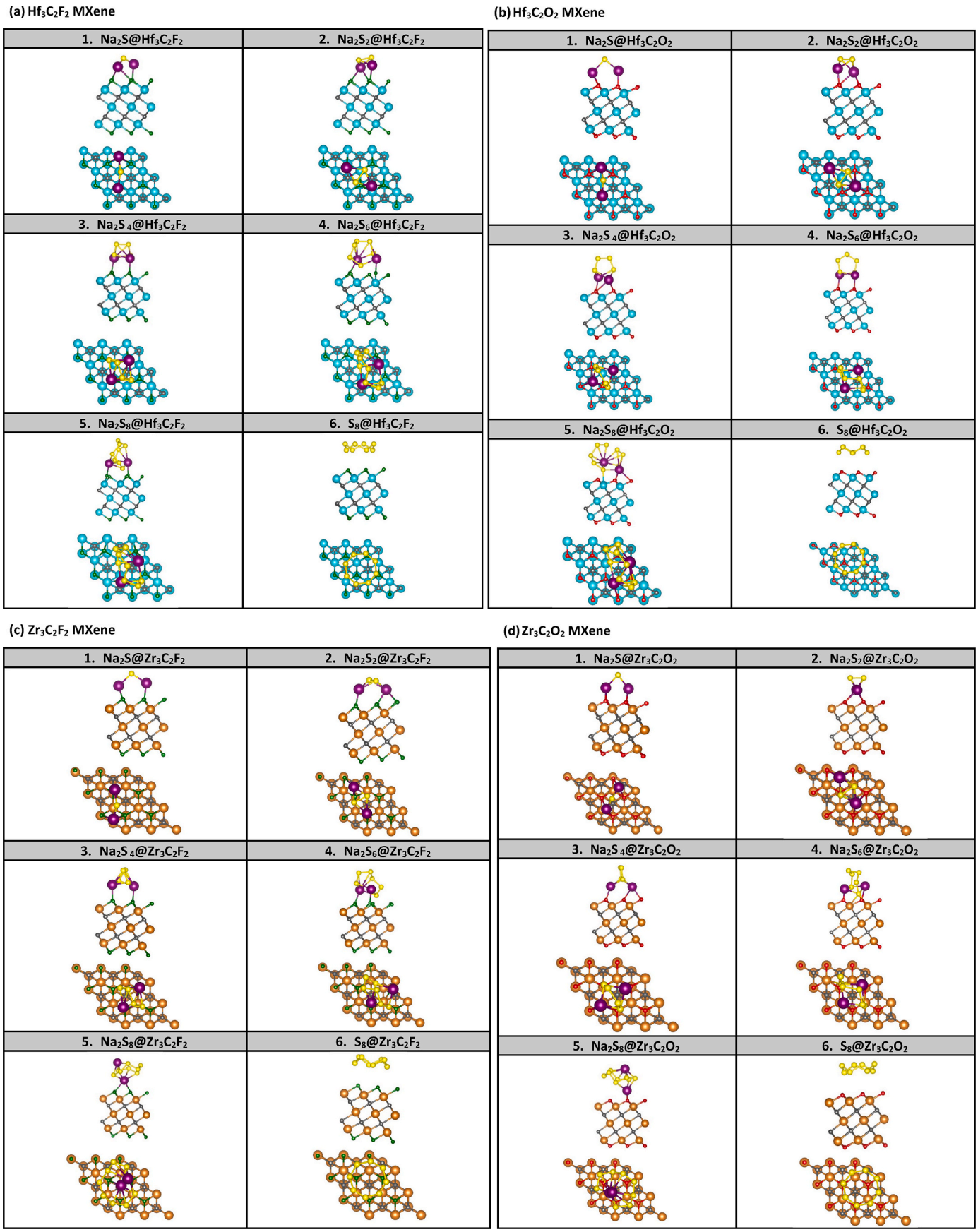

Fig. 3. Side and top views of relaxed 6 sodium polysulfides (Na_2S_n) adsorbed on four functionalized MXenes: (a) $Hf_3C_2F_2$, (b) $Hf_3C_2O_2$, (c) $Zr_3C_2F_2$, and (d) $Zr_3C_2O_2$.

Table 3
Distances between sodium polysulfides (Na_2S_n) and surfaces of 4 functionalized MXenes $Hf_3C_2T_2$ and $Zr_3C_2T_2$ (T = F,O).

System	Na_2S	Na_2S_2	Na_2S_4	Na_2S_6	Na_2S_8	S_8
$Hf_3C_2F_2$	2.121 Å	2.238 Å	2.326 Å	2.263 Å	2.226 Å	3.243 Å
$Hf_3C_2O_2$	2.279 Å	2.284 Å	2.282 Å	2.363 Å	2.393 Å	3.542 Å
$Zr_3C_2F_2$	2.293 Å	2.326 Å	2.363 Å	2.274 Å	2.384 Å	3.298 Å
$Zr_3C_2O_2$	2.001 Å	2.117 Å	2.178 Å	2.199 Å	2.236 Å	3.490 Å

3.2. Adsorption of Na_2S_n

Na_2S_n molecules were introduced on the surfaces of four MXenes to quantify the anchoring capabilities of the latter. The results of binding energies are shown in Fig. 2a and compared with those of electrolytes (DOL and DME). Fig. 2b compares the binding energies of Na_2S_n among the four MXenes that were analyzed in this study. Whereas Table 2 shows an extended comparison of our results of binding energies to others existing in literature. The oxygen passivated MXenes display the strongest binding energies which are competitive to those displayed for C_2N-based anchoring material [16,18–25].

In the study of adsorption, an initial assessment of the position and orientation of each of the polysulfides have been undertaken and different sites on the surface of MXene have been considered (see Fig. S1). Na_2S_n were exposed to MXene substrates by first orienting them closer to the functional group (F/O) marked by spot A, and then by placing them closer to the gap between two functional groups marked by spot B (i.,e., a top intermediate site between three A sites). The reported values of binding energy are the ones corresponding to fully relaxed molecules, which are a bit large and extend between or beyong two sites. Also, the sodium polysulfides (Na_2S, Na_2S_2, Na_2S_4, Na_2S_6, Na_2S_8) and S_8 molecule were first relaxed with sodium atoms aligned downwards, and then with their sulfur atoms aligned downwards at both the testing sites. The relaxed structures presented in Fig. 3a-d show the most stable and energetically favorable positions. For the S_8 molecule, since it comprises of only 1 element sulfur, it was relaxed only in the horizontal and vertical alignments and the most stable orientation has been presented in the Fig. 3a-d.

During the process of atomic relaxation, different potential locations and orientations of the exposed molecules were tested to identify the most energetically favorable sites and positions. The most strongly bound configurations of Na_2S_n on $Hf_3C_2F_2$, $Hf_3C_2O_2$, $Zr_3C_2F_2$, and $Zr_3C_2O_2$ are illustrated in Fig. 3(a–d). After the atomic relaxation process, S_8 prefers a horizontal alignment over the substrate, for all the four functionalized MXenes. This has also been observed for other 2D materials (e.g., As_2S_3 [21], black phosphorene [42], $Ti_3C_2T_x$ [43], graphene [44]). The distances between the S8 molecule and the MXenes are as follows: $Hf_3C_2F_2$ (O_2): 3.24 Å (3.542 Å) and $Zr_3C_2F_2$ (O_2): 3.29 Å (3.51 Å). These distances are greater than the sum of the atomic radii of S (1.00 Å) and F (0.42 Å)/O (0.66 Å) atoms, indicating that the binding is weak and is primarily due to van der Waals (vdW) interactions.

In the meantime, additional Na_2S_n molecules adhere to the MXenes by leading their Na atoms towards the functional group atoms F (O) atoms on the surface, as shown in Table 3, where the Na–F(O) distances are given. Bonding occurs between the Na_2S_n and the MXene substrate when the distance between the incoming molecule and the substrate is of the order of sum of the atomic radii of Na and F (O) (R_{Na} = 1.80 Å, R_F = 0.42 Å, R_O = 0.48 Å). The distances between Na_2S_n and $Hf_3C_2F_2$/$Hf_3C_2O_2$/$Zr_3C_2F_2$/$Zr_3C_2O_2$ are roughly equivalent to the sum of the radii of Sodium and Fluorine (Oxygen), indicating a strong chemical bond. These bonds can be tested experimentally by assessing their XPS spectra. The calculated binding energies (E_b) shown in Fig. 2a also support the strong binding, and the E_b values are compared to those of polysulfides adsorbed by commonly used electrolyte molecules such as 1,2-dimethoxyethane (DME) and 1,3-dioxolane (DOL) [25], as well as other 2D materials that have been proposed as anchoring materials in the literature. The interactions between all four MXenes are found to be significantly stronger than the Na_2S_n-electrolyte interactions, justifying the suppression of Na_2S_n dissolution in these electrolytes. Importantly, the moderate strength of interactions between Na_2S_n and the studied MXenes ensures the reversibility of the redox reaction.

The large values of E_b are due to the polarity of the surface F and O atoms. F (χ^F = 4.0 Pauling) [45] and O (χ^O = 3.5 Pauling) have much higher electronegativities than Hf (χ^{Hf} = 1.3 Pauling)/Zr (χ^F = 1.33 Pauling). As a result of this, the peripheral atoms present in the functional groups (Fluorine/Oxygen) attract electrons, thereby producing anions that directly attract the polar Na_2S_n analytes. As a result, an adhesive coating comprising of $Hf_3C_2F_2/O_2$ and $Zr_3C_2F_2/O_2$ on the cathode is sufficient to anchor the Na_2S_n molecules and effectively eliminate the shuttle effect.

It is a challenge to understand the nature of chemical bonding between Na_2S_n and the studied MXenes. This is primarily responsible for the suppression of these Na_2S_n molecules which cause the shuttle effect. However, we have determined that the van der Waals physical interactions play a significant role in the magnitude of the binding energies "E_b". We define the ratio of contribution of vdW interactions to the binding energy as follows:

$$R = \frac{E_b^{vdW} - E_b^{novdW}}{E_b^{vdW}} \times 100\% \quad (1)$$

where the notations, E_b^{vdW}, E_b^{novdW} represent the binding energies of Na_2S_n, with and without the inclusion of the van der Waals (vdW) interactions, respectively. Fig. 2b shows the ratio of the vdW energies of Na_2S_n adsorbed on the surfaces of $Hf_3C_2F_2$, $Hf_3C_2O_2$, $Zr_3C_2F_2$ and $Zr_3C_2O_2$ MXenes. Interestingly, intrinsic vdW interactions are the predominant contributors to the binding energy of S_8 on all the four MXenes which accounts for 83%, 64.96%, 75% and 62% of the binding energy for $Hf_3C_2F_2$, $Hf_3C_2O_2$, $Zr_3C_2F_2$ and $Zr_3C_2O_2$, respectively. Moreover, in the fluorine passivated MXenes, $Hf_3C_2F_2$ and $Zr_3C_2F_2$ the van-der-Waals interactions seem to be the controlling attractive force which accounts for the major contribution in the binding energies. This thereby justifies their relatively weaker interactions in comparison to their Oxygen-functionalized counterparts where the chemical binding energies seem to be significantly higher. Another key point to be noted, is that the vdW contributions appear to reduce with reductions in the sulfur content of the polysulfides, and therefore for Na_2S they reduce to only 54%, 25%, 51% and 23% for $Hf_3C_2F_2$, $Hf_3C_2O_2$, $Zr_3C_2F_2$ and $Zr_3C_2O_2$, respectively. This is justified by the presence of strong chemical bonds, and thereby an enhanced charge exchange between the Na_2S moiety and the MXenes as can be seen in the Bader charge transfer of Table 4. The transferred charge Δq from Na_2S_n to the passivation layer of MXenes increases with the reducing sulfur content of molecules and is also remarkably higher on oxygen passivation than fluorine passivation.

Aside of the physisorption of S_8 molecule on all the surfaces of

Table 4
Charge transferred from sodium polysulfides (Na_2S_n) to passivation layer of 4 studied MXene using Bader charge analysis within VASP package.

System	Na_2S	Na_2S_2	Na_2S_4	Na_2S_6	Na_2S_8	S_8
$Hf_3C_2F_2$	−0.38504	−0.37148	−0.06916	−0.17986	−0.174753	−0.02685
$Hf_3C_2O_2$	−0.876345	−0.87019	−0.8738503	−0.497036	−0.194004	−0.01494
$Zr_3C_2F_2$	−0.55453	−0.54979	−0.14118	−0.19513	−0.04056	−0.03028
$Zr_3C_2O_2$	−0.88898	−0.99504	−0.88124	−0.74342	−0.37673	−0.01511

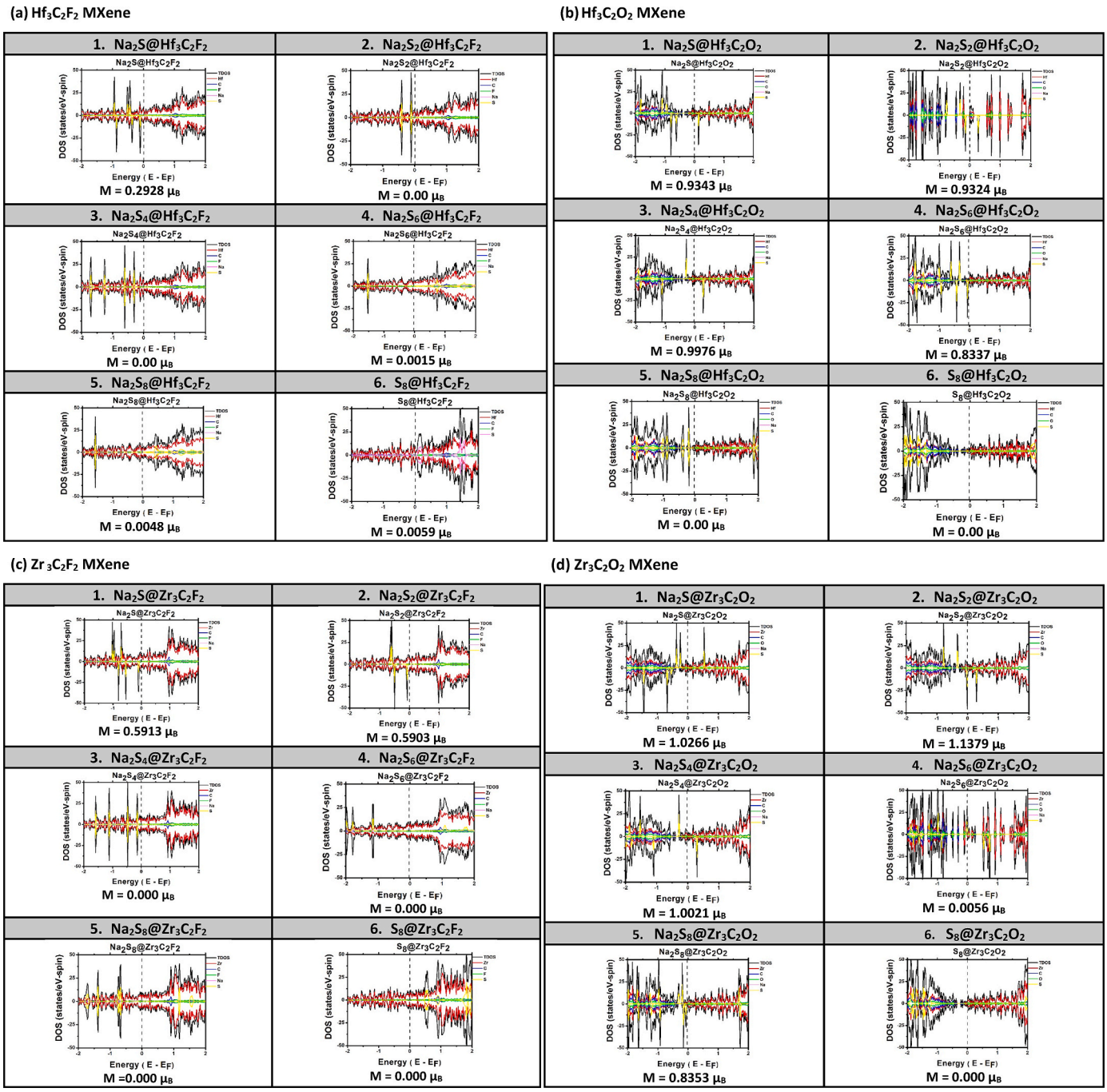

Fig. 4. Spin-polarized PDOS and TDOS of F/O-passivated MXenes after the adsorption of 6 sodium polysulfides: (a) $Hf_3C_2F_2$, (b) $Hf_3C_2O_2$, (c) $Zr_3C_2F_2$, and (b) $Zr_3C_2O_2$. Fermi level is taken as an energy reference ($E_F = 0$).

studied MXenes, the common trend amongst the adsorptions of the other five Na_2S_n is that they all exhibited chemisorption processes but not associated with molecular dissociation. Furthermore, in all cases both sodium atoms establish chemical bonds with the passivation layer of MXene except in three cases, corresponding to Na_2S_8 on $Zr_3C_2T_2$ (T = F/O) and Na_2S_6 on $Zr_3C_2O_2$ shown in Fig. 3c and d, respectively.

Afterwards, we investigated how the presence of Na_2S_n affects the intrinsic electronic properties of $Hf_3C_2F_2/O_2$ and $Zr_3C_2F_2/O_2$. Fig. 4 (a–d) depict the spin-polarized PDOS and TDOS of Na_2S_n adsorbed on $Hf_3C_2F_2$, $Hf_3C_2O_2$, $Zr_3C_2F_2$ and $Zr_3C_2O_2$ MXenes, respectively. The adsorption of the S_8 molecule did not produce any significant change in the TDOS of the MXenes, particularly near the Fermi energy, indicating that there is only a minor alteration in electronic properties such as electronic transport. This is in line with the weak nature of the bond, which is primarily physisorption involving weak van der Waals (vdW) attractive forces. However, significant changes occur in the total density of states (TDOS) when Na_2S_n is adsorbed, indicating significant binding energies and the presence of chemical bonding. However, the electronic properties of MXenes remain metallic after adsorption. Extra peaks in the short range around the Fermi energy suggest that the conductivity of the host is enhanced upon the availability of more conducting states. Some differences can be observed between the two spins (up/down) in some cases, such as $Hf_3C_2F_2$:Na_2S, $Hf_3C_2O_2$:Na_2S, Na_2S_2, Na_2S_4, Na_2S_6; $Zr_3C_2F_2$:Na_2S, Na_2S_2; and $Zr_3C_2O_2$:Na_2S, Na_2S_2, Na_2S_4, and Na_2S_8. However, the total magnetic moment remains small in comparison to the sample size. Therefore, overall, the adsorption of Na_2S_n has the

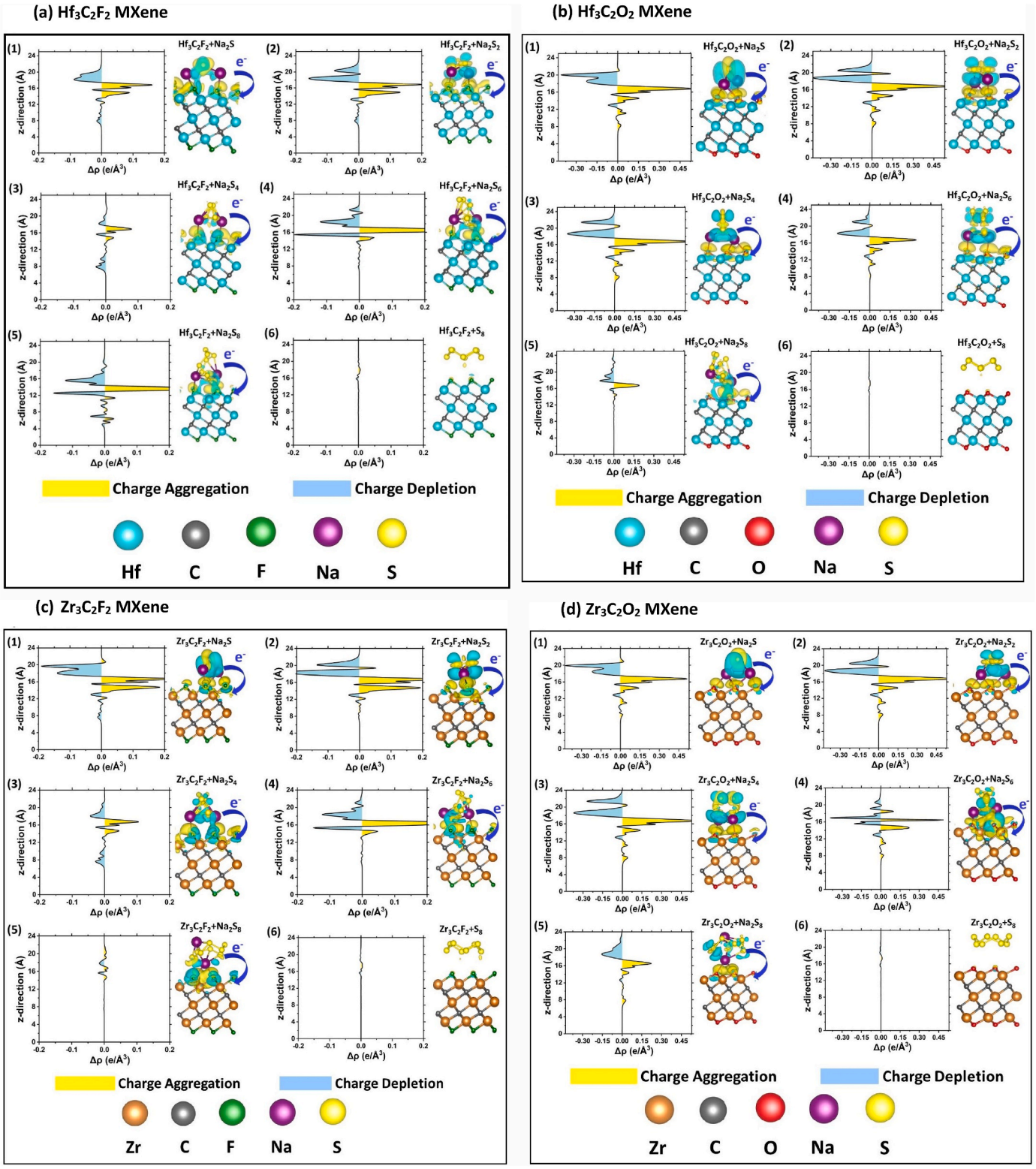

Fig. 5. Charge density difference (CDD) of sodium polysulfides (Na_2S_n) adsorbed on F/O-passivated MXenes: (a) $Hf_3C_2F_2$, (b) $Hf_3C_2O_2$, (c) $Zr_3C_2F_2$, and (b) $Zr_3C_2O_2$. The isosurface is set to be 0.003 e $Å^{-3}$. Both 3D plots and their projection on z-axis are shown.

potential to improve the electronic conduction property of the host materials. Furthermore, the metallicity is retained throughout the process of adsorption of the sodium polysulfides. The fact that there are additional electronic conduction states present around the Fermi energy and that the metallic feature is maintained means that there is conductive anchoring, which speeds up the electrochemical process while the battery is in operation.

3.3. Charge density difference (CDD)

Charge transfer is calculated by using Bader analysis with results shown in Table 4. As shown in this table, charge is donated from the

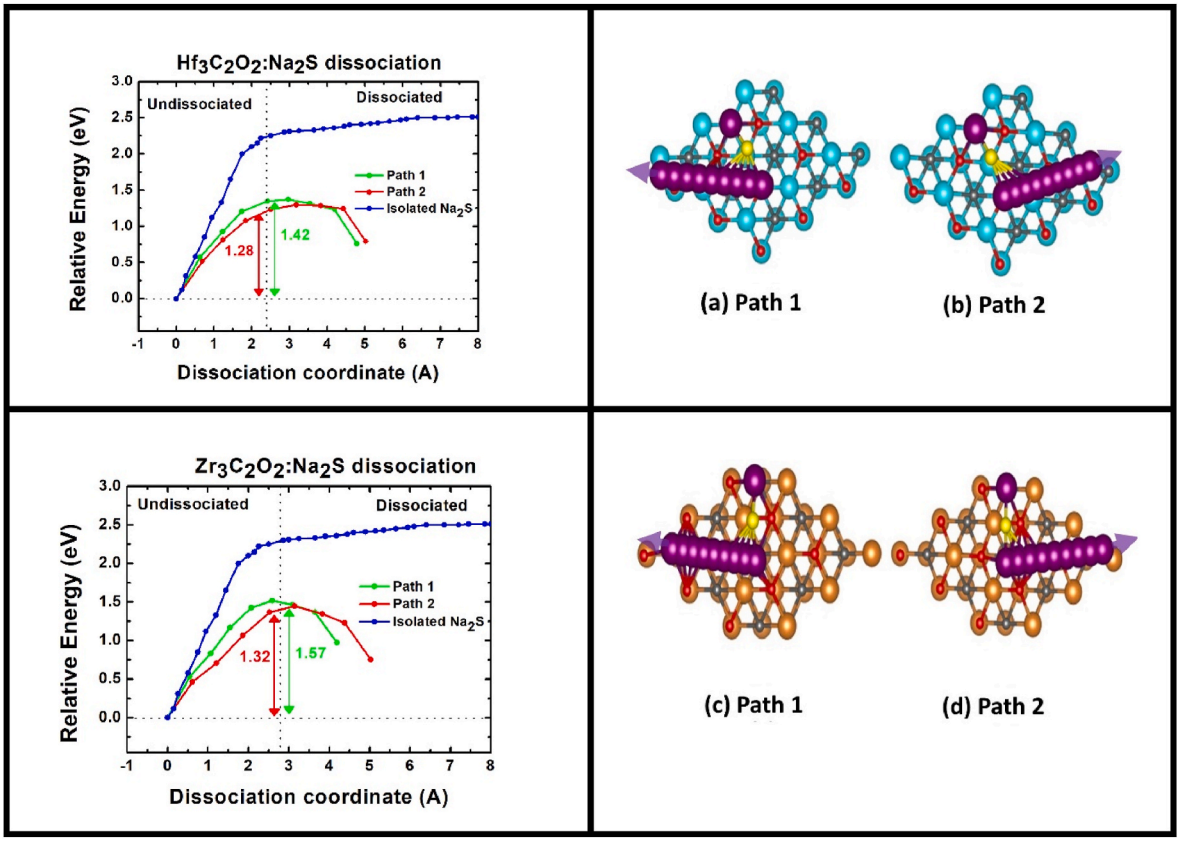

Fig. 6. Climbing image-nudged elastic band (CI-NEB) method to describe the dissociation molecule ($Na_2S \rightarrow NaS + Na^+ + e^-$) and the diffusion of Na + ion along 2 different paths on the surfaces of O-passivated Hf_3C_2 and Zr_3C_2 MXenes. Energy reference is at the start of dissociation process. The dissociation of free (Na_2S) molecule is shown in blue curve for a reference. Path #1 is from center of sample towards the left side; whereas path #2 is from center of sample towards the right side of it. (For interpretation of the references to color in this figure legend, the reader is referred to the Web version of this article.)

Na_2S_n to the MXenes. This charge donation was higher in case of O_2 functionalization of the Mxenes, in cases of chemisorption processes, which agrees with their stronger binding energies. In the case of S_8 molecule, charge transfer was negligible owing to their weak interaction and insignificant change on the density of states after adsorption. We computed the variation in charge density (CDD = $\Delta\rho$), using the given formula

$$\Delta\rho = \rho_{MXene+NPSs} - (\rho_{MXene} + \rho_{NPSs}) \quad (2)$$

Fig. 5(a–d) show the results of CDD corresponding to $Hf_3C_2F_2$, $Hf_3C_2O_2$, $Zr_3C_2F_2$ and $Zr_3C_2O_2$ MXenes, respectively. In Fig. 5, we display the charge density in both 3D and its projection (1D) on the z-axis. It seems that there is an accumulation of charge (represented by the color yellow) on the MXenes surface, and a decrease in charge (represented by the color cyan) on polysulfide clusters. This transfer of electrons is due to the movement of electrons from Na_2S_n's Na-3s to the partly filled 2p orbitals of the anchoring groups (Oxygen/Fluorine). It is important to note that the charge transfer is greater with oxygen passivation and decreases as the sulfur content in sodium polysulfides increases (Fig. 5b and d). In addition, the charge transfer is almost insignificant when S_8 is adsorbed, which is consistent with the results of Bader analysis and can be attributed to weak vdW-like interactions with the substrate. One last remark about the ρ(z), plots presented in Fig. 5, is that the wiggling at the interfacial region between the molecule and the MXene's surface should reveal the formation of covalent bonds.

3.4. Activation barrier

A crucial element for improving the ability of a battery to be recharged and for extending its lifespan is the catalytic conversion of the non-soluble by-product Na_2S into its oxidized form. To speed up the reaction kinetics, efforts are being made to reduce the dissociation barrier. This is calculated by using the climbing image-nudged elastic band (CI-NEB) method [46]. The dissociation process heavily relies on how fast the Na–S bonds break down on the anchors, which involves the dissociation of Na_2S. The electrocatalytic performance of RT-NSBs is limited due to a significantly high decomposition barrier. The study focused on the decomposition barriers of Na_2S on the most likely meta-stable states of the MXenes, specifically $Hf_3C_2O_2$ and $Zr_3C_2O_2$. The Na_2S moiety undergoes breakdown into two parts, an NaS cluster and an Na^+ ion ($Na_2S \rightarrow NaS + Na^+ + e^-$). Then, the freed Na^+ ion can move along two different paths on $Hf_3C_2O_2$ and $Zr_3C_2O_2$, and the potential barrier was determined along each path, as shown in Fig. 6. Path #1 is from center of sample towards the left whereas path #2 is from center of sample towards the right. The dissociation threshold of an individual Na_2S molecule serves as a basis for comparison, where the Na^+ ion that is freed is regarded as the origin on the dissociation coordinates' (x-axis). When the dissociation distance reaches 2.25 Å, the ion is regarded as being fully released [25]. The results show that Na_2S is much more energetic to dissociate on $Hf_3C_2O_2$ than $Zr_3C_2O_2$ due to its lower potential barrier on both paths (1.28 eV, 1.42 eV) and (1.32 eV, 1.57 eV) for $Hf_3C_2O_2$ and $Zr_3C_2O_2$, respectively. Both $Hf_3C_2O_2$ and $Zr_3C_2O_2$ greatly reduce the energy required for Na_2S dissociation as compared to an isolated Na_2S. Additionally, dissociating Na_2S is a spontaneous process on both $Hf_3C_2O_2$ and $Zr_3C_2O_2$ without the need for energy absorption. The resulting barriers are comparable with those of other 2-dimensional materials like single-layer vanadium disulfide (VS_2) 0.53 eV [46], chromium decorated nitrogen-doped graphene (Cr@NG) 1.54 eV [47], pure graphene 1.94 eV and Fe–N_4@ graphene 1.05 eV [48].

4. Conclusions

Spin-polarized DFT calculations were applied to explore a novel route of enhancing the performance and lifespan of the sodium-sulfur batteries by reducing the shuttle effect. This research demonstrates that MXenes (specifically $Hf_3C_2T_2$ and $Zr_3C_2T_2$ with T = F/O) are promising candidates for additive cathodes to efficiently suppress the shuttle effect and catalyze the electrochemical process. The results showed that the binding energies of sodium polysulfides (Na_2S_n) on all studied MXenes were stronger than those with electrolytes like DOL and DME. The study also found that oxygen passivation had a greater chemical binding effect on polysulfides to inhibit the shuttle effect (during the discharging phase) and lower the activation energy for ion kinetics (during the charging phase). These findings support the use of MXenes as additive cathodes in room-temperature sodium-sulfur batteries to improve their performance and extend their lifespan.

Data access statement

The information backing up the conclusion of this investigation can be obtained by contacting the authors through a reasonable request.

Ethics statement

The writers have verified that they have reviewed and comprehended the journal's guidelines and policies regarding research ethics and integrity.

CRediT authorship contribution statement

Saba Khan: Supervision, Software, Writing – review & editing, the primary author of this paper, conducted DFT calculations using the VASP software and plotted the Figures, contributed to the writing and the correction of the manuscript. supervisor, reviewed and edited the Figures, and authored the initial version of the manuscript. Consequently, their involvement in the present work can be categorized in the following proportions: 50%, 20%, 15%, and 15%. **Narender Kumar:** Supervision, Software, Writing – review & editing, contributed into the DFT Calculations, contributed to the writing and the correction of the manuscript. supervisor, reviewed and edited the Figures, and authored the initial version of the manuscript. Consequently, their involvement in the present work can be categorized in the following proportions: 50%, 20%, 15%, and 15%. **Tanveer Hussain:** Supervision, co-supervised the Ph.D. students and contributed to the writing and the correction of the manuscript. **Nacir Tit:** Supervision, Writing – review & editing, served as the PhD students' supervisor, reviewed and edited the Figures, and authored the initial version of the manuscript. Consequently, their involvement in the present work can be categorized in the following proportions: 50%, 20%, 15%, and 15%.

Declaration of competing interest

The authors declare that they have no known competing financial interests or personal relationships that could have appeared to influence the work reported in this paper.

Data availability

Data will be made available on request.

Acknowledgements

The authors would like to express their gratitude to Dr. Thomas Fowler for carefully reviewing the initial draft of the paper and to the National Water and Energy Center (NWEC) at the UAE University for sponsoring the research (Grant numbers: 12R125 and 12R162).

Appendix A. Supplementary data

Supplementary data to this article can be found online at https://doi.org/10.1016/j.jpowsour.2023.233298.

References

[1] M. Li, J. Lu, Z. Chen, K. Amine, 30 years of lithium-ion batteries, Adv. Mater. 30 (2018), 1800561.
[2] V. Etacheri, R. Marom, R. Elazari, G. Salitra, D. Aurbach, Challenges in the development of advanced Li-ion batteries: a review, Energy Environ. Sci. 4 (2011) 3243–3262.
[3] A. Fotouhi, D.J. Auger, K. Propp, S. Longo, M. Wild, A review on electric vehicle battery modelling: from Lithium-ion toward Lithium-Sulphur, Renew. Sustain. Energy Rev. 56 (2016) 1008–1021.
[4] M.D. Slater, D. Kim, E. Lee, C.S. Johnson, Sodium-ion batteries, Adv. Funct. Mater. 23 (2013) 947–958.
[5] R. Rajagopalan, Y. Tang, X. Ji, C. Jia, H. Wang, Advancement and challenges in potassium-ion batteries: a comprehensive review, Adv. Funct. Mater. 30 (2020), 1909486.
[6] N. Jayaprakash, S.K. Das, L.A. Archer, The rechargeable aluminum-ion battery, Chem. Commun. 47 (2011) 12610–12612.
[7] Y. Li, H. Dai, Recent advances in zinc-air batteries, Chem. Soc. Rev. 43 (2014) 5257–5275.
[8] Y.X. Wang, B. Zhang, W. Lai, Y. Xu, S.L. Chou, H.K. Liu, S.X. Dou, Room-temperature Sodium-Sulfur batteries: a comprehensive review on research progress and cell chemistry, Adv. Energy Mater. 7 (2017), 1602829.
[9] Y. Wang, D. Zhou, V. Palomares, D. Shanmukaraj, B. Sun, X. Tang, C. Wang, M. Armand, T. Rojo, G. Wang, Revitalising sodium-sulfur batteries for non-high-temperature operation: a crucial review, Energy Environ. Sci. 13 (2020) 3848–3879.
[10] D. Kumar, S.K. Rajouria, S.B. Kuhar, D.K. Kanchan, Progress and prospects of sodium-sulfur batteries: a review, Solid State Ionics 312 (2017) 8–16.
[11] X. Xu, D. Zhou, X. Qin, K. Lin, F. Kang, B. Li, D. Shanmukaraj, T. Rojo, M. Armand, G. Wang, A room-temperature sodium-sulfur battery with high capacity and stable cycling performance, Nat. Commun. 9 (2018) 3870.
[12] Y. Tian, et al., Promises and challenges of next –generation "Beyond Li-ion" batteries for electric vehicles and grid decarbonization, Chem. Rev. 121 (2021) 1623–1669.
[13] R. Fang, J. Xu, D.W. Wang, Covalent fixing of sulfur in metal-sulfur batteries, Energy Environ. Sci. 13 (2020) 432–471.
[14] P. Hu, F. Xiao, Y. Wu, X. Yang, N. Li, H. Wang, J. Jia, Covalent encapsulation of sulfur in a graphene/N-doped carbon host for enhanced sodium-sulfur batteries, Chem. Eng. J. 443 (2022), 136257.
[15] F. Xiao, X. Yang, H. Wang, J. Xu, Y. Liu, D.Y.W. Yu, A.L. Rogach, Covalent encapsulation of sulfur in a MOF-derived S,N-doped porous carbon host realized via vapor-infiltration method: results in enhanced Sodium-Sulfur battery performance, Adv. Energy Mater. 10 (2020), 2000931.
[16] T. Hussain, T. Kaewmaraya, Z. Hu, X.S. Zhao, Efficient control of the shuttle effect in sodium-sulfur batteries with functionalized nanoporous graphenes, ACS Appl. Nano Mater. 5 (2022) 12637–12645.
[17] F. Xiao, H. Wang, J. Xu, W. Yang, X. Yang, D.Y.W. Yu, A.L. Rogach, Generating short-chain sulfur suitable for efficient Sodium-Sulfur batteries via atomic copper sites on N,O-codoped carbon composite, Adv. Energy Mater. 11 (2021), 2100989.
[18] T. Zhang, Z. Chen, J. Zhao, Y. Ding, Metal-N4/graphene as an efficient anchoring material for lithium-sulfur batteries: a computational study, Diam. Relat. Mater. 90 (2018) 72–78.
[19] Z. Yan, Y. Liang, W. Hua, X.-G. Zhang, W. Lai, Z. Hu, W. Wang, J. Peng, S. Indris, Y. Wang, S.-L. Chou, H. Liu, S.-X. Dou, Multiregion Janus-featured cobalt phosphide-cobalt composite for highly reversible room-temperature sodium-sulfur batteries, ACS Nano 14 (2020) 10284–10293.
[20] M. Sajjad, T. Hussain, N. Singh, J.A. Larsson, Superior anchoring of sodium polysulfides to the polar C_2N 2D material: a potential electrode enhancer in sodium–sulfur batteries, Langmuir 36 (2020) 13104–13111.
[21] T. Kaewmaraya, T. Hussain, R. Umer, Z. Hu, X.S. Zhao, Efficient suppression of the shuttle effect in Na-S batteries with an As_2S_3anchoring monolayer, Phys. Chem. Chem. Phys. 22 (2020) 27300–27307.
[22] N. Wang, Y. Wang, Z. Bai, Z. Fang, X. Zhang, Z. Xu, Y. Ding, X. Xu, Y. Du, S. Dou, G. Yu, High-performance room-temperature sodium-sulfur battery enabled by electrocatalytic sodium polysulfides full conversion. Ene, Environ. Sci. 13 (2020) 562–570.
[23] W. Bao, C.E. Shuck, W. Zhang, X. Guo, Y. Gogotsi, G. Wang, Boosting performance of Na–S batteries using sulfur-doped $Ti_3C_2T_x$ MXene nanosheets with a strong affinity to sodium polysulfides, ACS Nano 13 (2019) 11500–11509.
[24] P. Ma, D. Fang, Y. Liu, Y. Shang, Y. Shi, H.Y. Yang, MXene-based materials for electrochemical Sodium-ion storage, Adv. Sci. 8 (2021), 2003185.
[25] N. Thatsami, P. Tangpakonsab, P. Moontragoon, R. Umer, T. Hussain, T. Kaewmaraya, Two-dimensional titanium carbide ($Ti_3C_2T_x$) MXenes to inhibit the shuttle effect in sodium-sulfur batteries, Phys. Chem. Chem. Phys. 24 (2022) 4187–4195.
[26] Z. Wang, Y. Zhang, H. Jiang, C. Wei, Y. An, L. Tan, S. Xiong, J. Feng, Free-standing $Na_2C_6O_6$/MXene composite paper for high-performance organic sodium-ion batteries, Nano Res. 16 (2023) 458–465.

[27] M. Naguib, M. Kurtoglu, V. Presser, J. Lu, J. Niu, M. Heon, L. Hultman, Y. Gogotsi, M.W. Barsoum, Two-dimensional nanocrystals produced by exfoliation of Ti_3AlC_2, Adv. Mater. 23 (2011) 4248–4253.
[28] M. Alhabeb, K. Maleski, B. Anasori, P. Lelyukh, L. Clark, S. Sin, Y. Gogotsi, Guidelines for synthesis and processing of two-dimensional titanium carbide ($Ti_3C_2T_x$ MXene), Chem. Mater. 29 (2017) 7633–7644.
[29] M. Sadiq, L. Pang, M. Johnson, V. Sathish, Q. Zhang, D. Wang, 2D nanomaterial, Ti_3C_2 MXene-based sensor to guide lung-cancer therapy and management, Biosensors 11 (2021) 40.
[30] X.H. Wen, X.F. Zhao, X.H. Wang, Y. Wang, J.C. Guo, H.G. Zhou, C.T. Zuo, H.L. Lu, Fe_3O_4/MXene nanosphere-based microfluidic chip for the accurate diagnosis of Alzheimer disease, ACS Appl. Nano Mater. 5 (2022) 15925–15933.
[31] H. Liu, W.H. Lai, Y. Lei, H. Yang, N. Wang, S. Chou, H.K. Liu, S.X. Dou, Y.X. Wang, Electrolytes/Interphases: Enabling distinguishable sulfur redox processes in room-temperature sodium-sulfur batteries, Adv. Energy Mater. (2022), 2103304.
[32] J. Zhou, et al., Synthesis and electrochemical properties of two-dimensional Hafnium Carbide, ACS Nano 11 (2017) 3841–3850.
[33] J. Zhou, X. Zha, F.Y. Chen, Q. Ye, P. Eklund, S. Du, Q. Huang, A new two-dimensional Zirconium Carbide MXene by selective etching of Al_3C_3 from nanolaminated $Zr_3Al_3C_5$, Angew. Chem. 55 (2016) 5008–5013.
[34] M. Tang, J. Li, Y. Wang, W. Han, S. Xu, M. Lu, W. Zhang, H. Li, Surface terminations of MXene: synthesis, characterization, and properties, Symmetry 14 (2022) 41, 2232.
[35] J. Hafner, Ab-initio simulations of materials using VASP: density-functional theory and beyond, J. Comput. Chem. 29 (2008) 2044–2078.
[36] M. Ernzerhof, G.E. Scuseria, Assessment of the Perdew-Burke-Ernzerhoff exchange-correlation functional, J. Chem. Phys. 110 (1999) 5029.
[37] H.J. Monkhorst, J.D. Pack, Special points for Brillouin-zone integrations, Phys. Rev. B 13 (1976) 5188–5192.
[38] S. Grimme, J. Antony, S. Ehrlich, H. Krieg, A consistent and accurate ab-initio parametrization of density functional dispersion correction (DFT-D) for the 94 elements H-Pu, J. Chem. Phys. 132 (2010), 154104, 19pp.
[39] G. Henkelman, A. Arnaldsson, H. Jonsson, A fast and robust algorithm for Bader decomposition of charge density, Comput. Mater. Sci. 36 (2006) 354–360.
[40] Z. Yang, Y. Zheng, W. Li, J. Zhang, Investigation of two-dimensional Hf-based MXenes as the anode materials for Li/Na-Ion batteries: a DFT study, J. Comput. Chem. 40 (2019) 1352–1359.
[41] Q. Meng, Z. Lo, J.L. Ma, A. Hu, Theoretical Investigation of Zirconium Carbide MXenes as prospective high-capacity anode materials for Na-ion batteries, J. Mater. Chem. A 6 (2018), 13652.
[42] H.H. Haseeb, Y. Li, S. Ayub, Q. Fang, L. Yu, K. Xu, F. Ma, Defective phosphorene as a promising anchoring material for lithium–sulfur batteries, J. Phys. Chem. C 124 (2020) 2739–2746.
[43] D. Wang, F. Li, R. Lian, J. Xu, D. Kan, Y. Liu, G. Chen, Y. Gogotsi, Y. Wei, A general atomic surface modification strategy for improving anchoring and electrocatalysis behavior of $Ti_3C_2T_2$ MXene in lithium-sulfur batteries, ACS Nano 13 (2019) 11078–11086.
[44] Z. Du, X. Chen, W. Hu, C. Chuang, S. Xie, A. Hu, W. Yan, X. Kong, X. Wu, H. Ji, L. J. Wan, Cobalt in nitrogen-doped graphene as single-atom catalyst for high-sulfur content lithium-sulfur batteries, J. Am. Chem. Soc. 141 (2019) 3977–3985.
[45] L. Pauling, The nature of the chemical bond. IV. The energy of single bonds and the relative electronegativity of atoms, J. Am. Chem. Soc. 54 (1932) 3570–3582.
[46] K. Yang, D. Liu, Y. Sun, Z. Qian, S. Zhong, R. Wang, Metal-N_4@Graphene as multifunctional anchoring materials for Na-S batteries: first-principles study, Nanomaterials 11 (2021) 1197.
[47] R. Jayan, M.M. Islam, Single-atom catalysts for improved cathode performance in Na–S batteries: a density functional theory (DFT) study, J. Phys. Chem. C 125 (2021) 4458–4467.
[48] G. Henkelman, B.P. Uberuaga, H. Jonsson, A climbing image nudged elastic band method for finding saddle points and minimum energy paths, J. Chem. Phys. 113 (2000) 9901–9904.